Geosciences 2021, 11(1): 1-9
DOI: 10.5923/j.geo.20211101.01

SAR Images Denoising Using Bidimensional Variational Mode Decomposition and Nonlocal Means Reprojection with Minimizing Variance

Harouchi Badre[1], Yassine Tounsi[2,*], Mohammed Said Rachafi[1], Hamid Bioud[2], Abdelkrim Nassim[2]

[1]Research Group for Applied Physics, Abdelmalek Essaadi University, Sciences and Technologies Faculty, Tangier, Morocco
[2]Control and Instrumentation Measurement Laboratory Chouaib Doukkali University, Faculty of Sciences, El Jadida, Morocco

Abstract Synthetic aperture radar (SAR) is very high and accurate technology for remote sensing. SAR images are very exploited for change detection and monitoring because of their high resolution. Because of the coherent retro diffusion of the backscattered radar waves with the rigorous earth surface, SAR images are characterized by a multiplicative noise called speckle that influences their analysis. For this reason, this paper aims to exploit the two-dimensional variational mode decomposition and combines it with the nonlocal means reprojection method to denoise SAR images. The proposed method concerns to decompose the SAR image into a series of variational mode functions called S-D IMFs and N-D IMFs, however, the speckle noise is high-frequency information, which means that it is concentrated in N-D IMFs components. Then, the denoising of N-D IMFs components is implemented using NLM reprojection using box kernel with minimizing variance. Firstly, we use numerical simulation to study the performance of our method, this study concerns use several synthetic images and add speckle noise for different variance, and then we apply the proposed method. The quantitative appraisal will be realized using three important metrics such as peak signal to noise ratio (PSNR), Edge preservation index (EPI), and image quality index (Q). Also, we compare our proposed method with other famous techniques as the Lee filter, Frost filter, and NLM-SAR method. Secondly, the proposed method will be exploited to denoise a real SAR image.

Keywords SAR image, Variational mode decomposition, Nonlocal mean reprojection, Speckle noise

1. Introduction

SAR images become a high and accurate tool for remote sensing dedicated to a large variety of applications [1]. The SAR sensors make the observation of the earth's surface with high resolution despite the weather conditions and sun phenomena [2]. Thanks to the advantages of SAR images and their numerous applications, research studies being actively conducted around the field of image filtering [3], image segmentation [4], image classification [5], image fusion [8-9], etc.

In contrast with the optical sensor, the SAR sensor is characterized by a coherent imaging system, and in the reason of earth surface roughness, a self-interference of the backscattering SAR waves from the earth surface is arised, and this is represented by high-frequency information in the SAR images called speckle noise.

Speckle noise is commonly observed in radar detection systems, although it can appear in any type of remote sensing image using coherent radiation. Like laser light, electromagnetic waves emitted by active sensors move in phase and have little interaction on their path to the target area. Reducing the effect of speckle noise allows both better discrimination of targets in the scene and easier automatic segmentation of the image.

Speckle noise is a multiplicative noise unlike Gaussian noise and salt-pepper noise and it has characterized by the Rayleigh distribution [7]. This noise can be modeled by multiplications of random values with the pixel values of the image and can be expressed as:

$$I_n(x,y) = I(x,y) * n(x,y) \quad (1)$$

Where $I_n(x,y)$ is the noised image, $I(x,y)$ is the clean image, and $n(x,y)$ represents the noise distribution.

Denoising is the process of reconstructing the original image by removing unwanted noise from a corrupted image. It is designed to reduce noise while preserving as much image structure and detail as possible. The main challenge is to design noise reduction filters that offer a compromise between these two elements.

* Corresponding author:
yassinetounsi132@gmail.com (Yassine Tounsi)
Received: Mar. 15, 2021; Accepted: Apr. 9, 2021; Published: Apr. 26, 2021
Published online at http://journal.sapub.org/geo

In general, image denoising approaches can be classified as spatial domain, transformation domain and dictionary learning depending on the image representation.

Spatial domain methods include local and non-local filters, which exploit similarities between pixels or patches in an image. Methods based on dictionary learning and transform domains contemplate transforming images into other domains, in which similarities of transformed coefficients are used. The difference between these two approaches is that transformation domain approaches generally use fixed basis functions to represent images, but learning-based methods use sparse representations on a redundant dictionary.

The spatial domain methods attempt to use the correlations that exist in most natural images [8]. For a given patch (pixel), a series of candidates will be used in the filtering process. Depending on the selection of candidates, spatial filters can be classified into local and non-local filters. A filter is considered local if the support of the filter is a spatial neighborhood of the candidate pixel and if the coefficients of the filter are limited by the spatial distance.

A large number of local filtering algorithms have been designed for noise reduction such as the Gaussian filter [9], the mean least squares filter, the entrained filter (TF), the bilateral filter, the anisotropic filtering [13-14].

In contrast, non-local filters use the self-similarity of natural images in a non-local way. Non-local means (NLM) [11-12] make it possible to obtain a denoised zone by calculating the weighted average of all the other zones of the same image.

The second category is that of the methods of the transformation domain using wavelets transform [13-17] and Fourier transform [18-19]. In each corresponding domain transform, the image is represented by coefficients, and the denoising process is realized by thresholding these coefficients and reconstructed using the corresponding inverse transform. Other transforms are also exploited for SAR images denoising as contourlet transform [20-21] and curvelet transform [22-23].

The third and final category of the denoising method is and hybrid method. The deep learning-based method becomes powerful in recent years and gives high-quality results [24-25]. Whereas, the hybrid methods are based on the combination of several methods in different denoising method categories [26-27].

In this work, an adaptation of Riesz wavelets transform is realized in order to make it suitable for SAR image denoising. This transform has given good results in digital speckle pattern interferometry [28-29], and this paper is an extension of this method for SAR images. The remaining of this work is as follows: The second part is focused on the description of the methodology of the proposed method, and the third section is dedicated to present the important finding and discussion.

2. Basic Theory of Bidimensional Variational Mode Decomposition

The VMD was introduced in 2014 by Dragomiretskiy & Zosso [30] for signal processing as a non-recursive alternative to the empirical mode decomposition (EMD) algorithm [31]. This technique has gained great interest in the field of signal analysis and processing [32-33]. The 2D-VMD algorithm is developed based on VMD theory for image decomposition [34], it can decompose an image into high and low-frequency components. The constrained variational equation in the 2D-VMD algorithm is expressed as follows:

$$\begin{cases} \min\limits_{u_k, w_k} \left\{ \sum\limits_k \alpha_k \left\| \nabla \left[u_{AS,k}(x) e^{-j\langle w_k, k\rangle} \right] \right\|_2^2 \right\} \\ s.t. \quad \forall x: \ \sum\limits_k u_k(x) = f(x) \end{cases} \tag{2}$$

where $u_{AS,k}(x)$ represents the analytic signal of the k^{th} mode. k is the number of decomposed IMFs. w_k is the central frequency of each sub-mode after decomposition, and $f(x)$ is the input image. In order to make the problem unconstrained, the quadratic penalty factor and Lagrange multiplier are introduced to enhance the fidelity. The augmented Lagrange expression can be formulated as:

$$\begin{aligned} L\left(\{u_k\}, \{w_k\}, \lambda\right) = & \sum_k \alpha_k \left\| \nabla \left[u_{AS,k}(x) e^{-j\langle w_k, k\rangle} \right] \right\|_2^2 \\ & + \left\| f(x) - \sum_k u_k(x) \right\|_2^2 + \left\langle \lambda(x), f(x) - \sum_k u_k(x) \right\rangle \end{aligned} \tag{3}$$

where λ is the Lagrange multiplier, α_k is the penalty factor, u_k is the set of modes, and w_k is the set of center frequencies. Then, the problem is transformed into that of solving the equation parameters shown as follows:

$$\min_{u_k, w_k} \max_{\lambda} L\left(\{u_k\}, \{w_k\}, \lambda\right). \tag{4}$$

Updating u_k^{n+1}, w_k^{n+1} and λ_k^{n+1}, one has:

$$u_k^{n+1}(w) = \left(f(w) - \sum_{i \neq k} u_i(w) + \frac{\lambda(w)}{2} \right) \frac{1}{1 + 2\alpha_k |w - w_k|^2}$$

$$\forall w \in \Omega_k : \Omega_k = \left\{ w \middle| \langle w, w_k \rangle \geq 0 \right\}, \tag{5}$$

$$w_k^{n+1} = \frac{\int_{\Omega_k} w |u_k(w)|^2 \, dw}{\int_{\Omega_k} |u_k(w)|^2 \, dw}, \tag{6}$$

$$\lambda^{n+1}(x) = \lambda^n(x) + \tau \left(f(x) - \sum_k u_k^{n+1}(x) \right). \tag{7}$$

The iteration terminating condition is given as follow:

$$\frac{\sum_k \left\| u_k^{n+1} - u_k^n \right\|_2^2}{\left\| u_k^n \right\|_2^2} < k\varepsilon. \quad (8)$$

From the Eq. Below, it can be obtained that the number of IMFs is K.

2.1. The Proposed Denoising Algorithm Based on 2D VMD and NLM Reprojection

The adopted methodology for SAR image denoising is shown by the flowchart presented in Figure 1. The first step concerns to decompose the input noised image into a series of variational mode functions using a two-dimensional variational mode decomposition algorithm. The algorithm decomposes a noised image into a series of S-D IMFs and N-D IMFs and a remaining part called residue as following:

$$X(x,y) = \sum_{i=1}^{m} IMF_i(x,y) + \sum_{m+1}^{N} IMF_i(x,y) + r(x,y) \quad (9)$$

It can be seen that the obtained IMFs can be classified into two families: the S-D IMFs (first term) containing image information, and the N-D IMFs containing the high-frequency information.

In the case of SAR images, speckle noise which is a high frequency and undesired information is concentrated in the N-D IMFs, consequently, the processing operation focus just on these components. In this work, we propose to use the NLM Reprojection method using box-kernel with minimizing variance reprojection because it showed a high capability to denoise fringe pattern and it is very fast [12].

An example of the decomposition of airplane image by 2D-VMD into four variational mode function is shown in Figure 2. Figure 2.a represents the input image and Figure 2(b-e) show the bidimentional IMFs obtained after the decomposition of input image (Figure 2.a) by 2D-VMD. The first IMF (Figure 2.b) contains the high frequency information wheras the final IMF (Figure 2.e) is a residue containing the low frequency information.

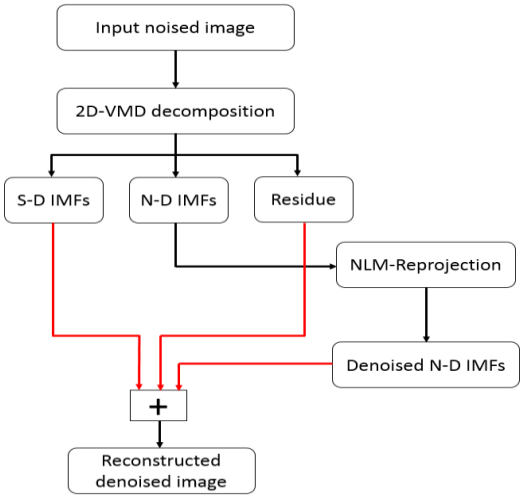

Figure 1. The flowchart of the proposed denoising algorithm

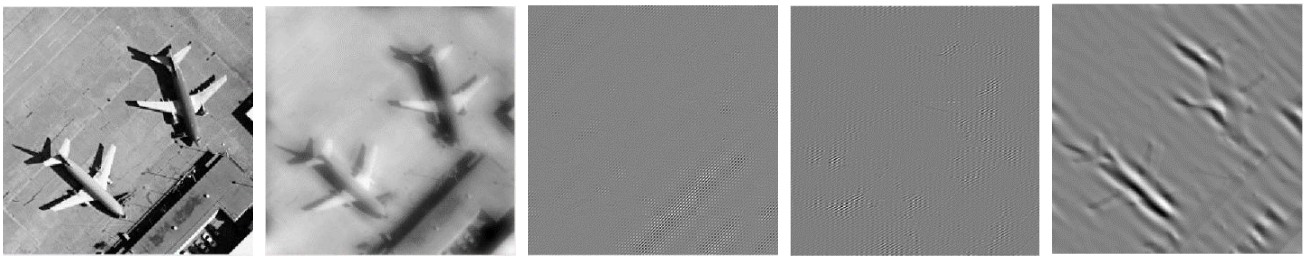

(a) (b) (c) (d) (e)

Figure 2. The sub-modes of the airplane image. (a) input image. (b) IMF1. (c) IMF2. (d) IMF3 and (e) IMF4

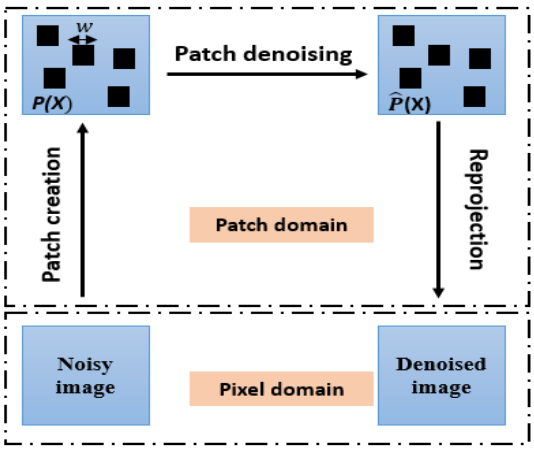

Figure 3. NLM reprojection scheme

Since the NLM method is based on the creation of a collection of patches, then each patch is denoised by taking into account the appropriate estimators such as a weighted average of the noisy patches based on the similarity among these patches, and the final information retrieved from these patch estimators is reprojected to the pixel space in order to recover the pixel estimators, as demonstrated in Figure 3.

There are several reprojection procedures to recover the pixelated denoised information from the denoised patches because the space of patches has a larger dimension than the original image space [35].

Consider w as the width of a patch. Since the patches overlap every pixel belongs to w^2 patches. Every patch in the image is estimated using a weighted average with the weights, $w(X, X')$ with $X = (x, y)$, and the filtered

estimator for any patch is given as

$$P(X) = \sum_{x' \in \Omega^{\dim}}^{\sum} x(X, X').P(X') \quad (10)$$

The minimizing Variance-Reprojection (*Mv*) is based on the patch selection and minimizing the expectation of the quadratic error between these selected patches. This requires choosing the estimator having minimal variance defined as

$$\hat{I}_{Mv} = P_{\delta}(\delta) \quad \text{with} \quad \delta = \arg\min Var\left(P_{\delta}(\delta)\right) \quad (11)$$

3. Results and Discussions

3.1. Numerical Simulation

The validation of the proposed method is done firstly using numerical simulation, this study concerns to use synthetic images and add speckle noise for differents variances *v* using the Matlab command '*imnoise (image, 'speckle',v)*. The use of different variances of speckle noise is important to show the behavior of the proposed technique in front of this parameter that represent the earth's surface rugosity.

(a) (b)

Figure 4. Input clean image using for performance study: (a) airplane, (b) building

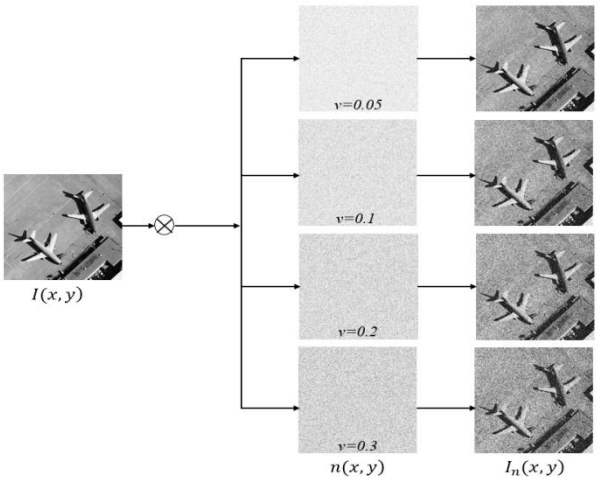

Figure 5. Procedure of numerical simulation data used in this work

The different synthetic images used in this study are shown in Figure 4 and represent the airplane and building images. Figure 5 shows the procedure used to generate the noisy image with different speckle noise variance *v={0.05; 0.1; 0.2; 0.3}.*

The noisy airplane and building images using the four variances of speckle are presented in Figure 6. The results of denoising for each speckle variance value using the proposed method is presented in Figure 7. To compare with the famous technique in literature, we choose Frost filter [36], Lee filter [37], and NLM-SAR method [38]. The reason for the choice of these three techniques for comparison is that the NLM-SAR method is considered as a powerful method for SAR image denoising, whereas, Lee and Frost's filter are two famous multi looking filter exploited in some software of radar image processing as SNAP (Sentinel Application Platform) developed by European Space Agency (ESA). The results of denoising the airplane and building images by Frost filter, Lee filter, and NLM-SAR method are presented in Figure 8, Figure 9, and Figure 10 respectively.

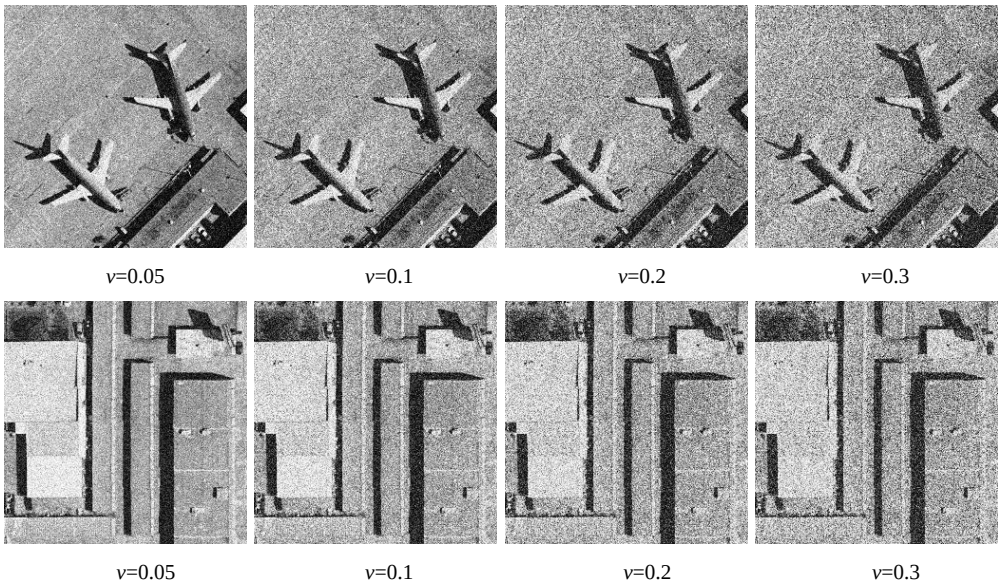

v=0.05 *v*=0.1 *v*=0.2 *v*=0.3

v=0.05 *v*=0.1 *v*=0.2 *v*=0.3

Figure 6. Noised airplane and building images by speckle noise with different variances

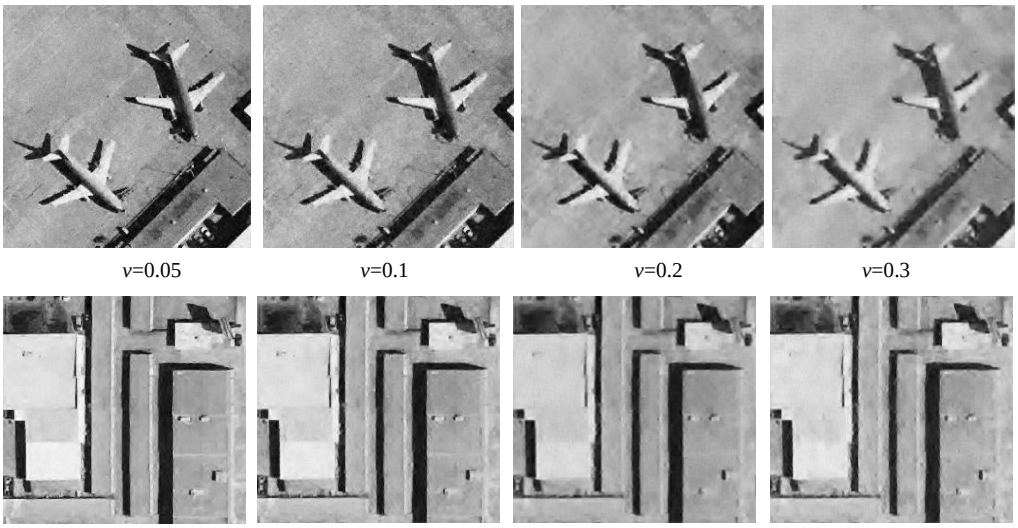

Figure 7. Denoised airplane and building images for each speckle noise variance using the proposed method

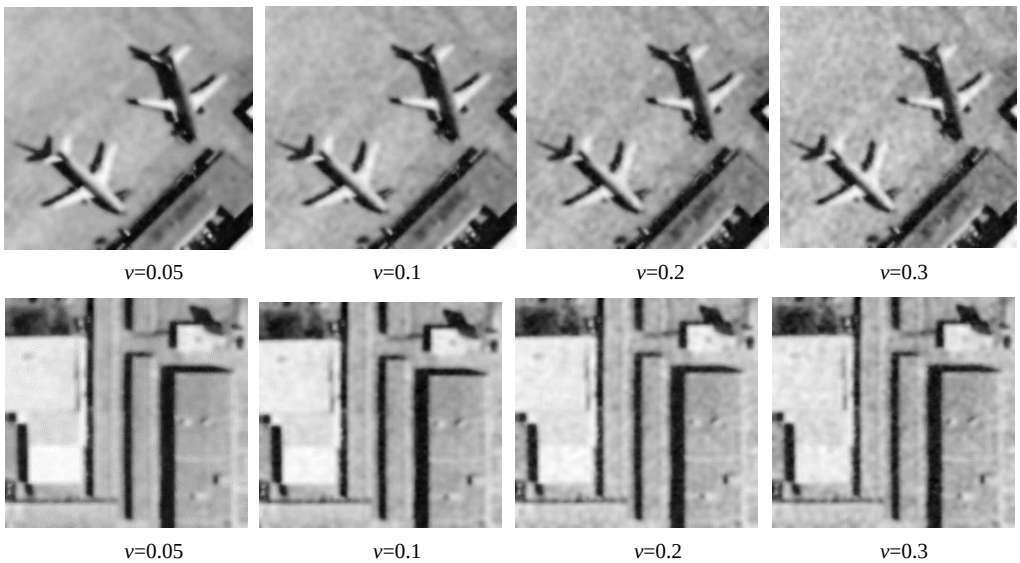

Figure 8. Denoised airplane and building images for each speckle noise variance using Frost filter

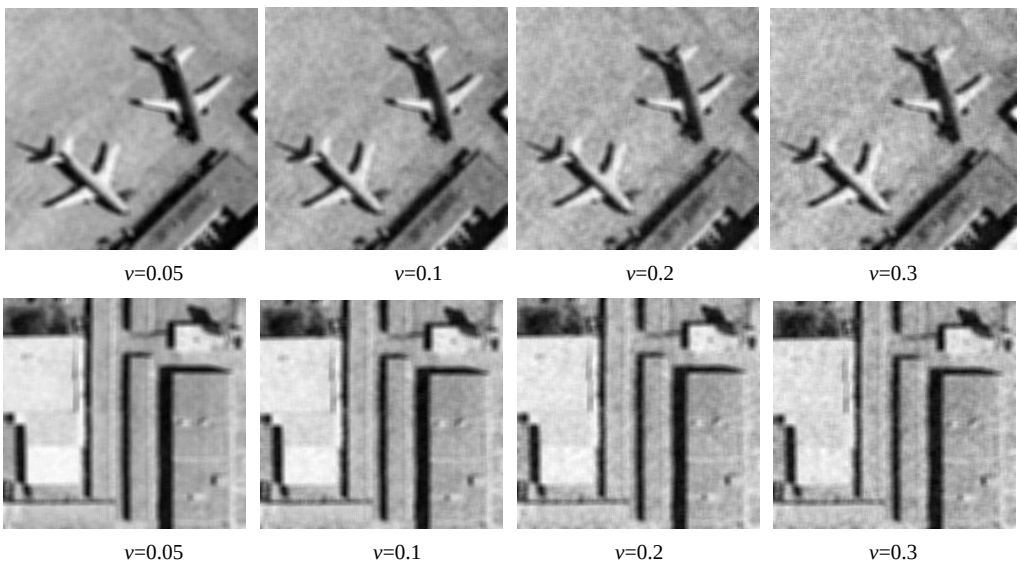

Figure 9. Denoised airplane and building images for each speckle noise variance using Lee filter

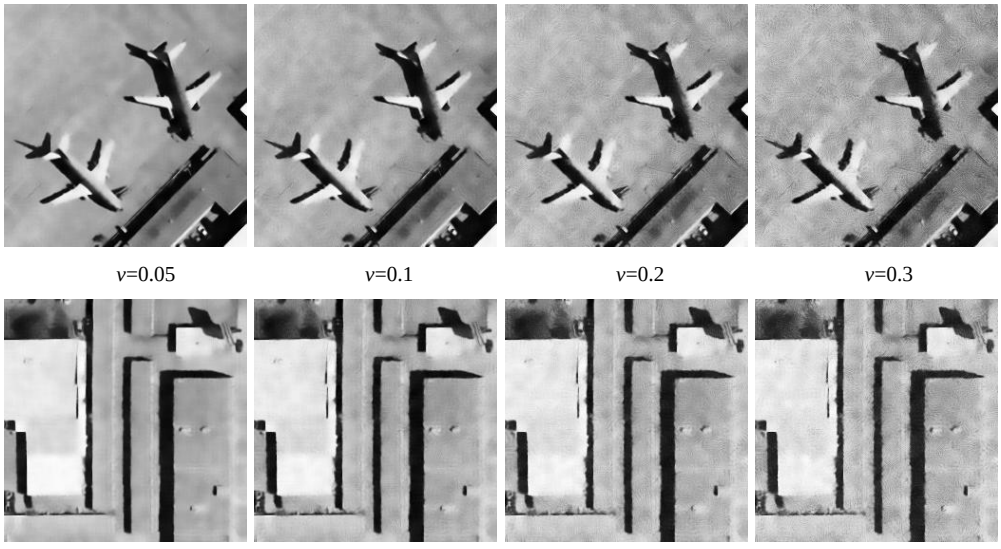

Figure 10. Denoised airplane and building images for each speckle noise variance using NLM-SAR method

3.2. Quantitative Appraisal

The effectiveness and assessment of a denoising method can be evaluated quantitatively by using several criteria metrics such as peak signal-to-noise ratio (*PSNR*), quality index (*Q*), edge preservation index (*EPI*), Signal-to-noise ratio (*SNR*), etc. Some of these criteria metrics are based on ground truths in which the obtained denoised image is compared with its corresponding noise-free image. On the other hand, some criteria metrics are termed blind metrics in which the measurement is based on the comparison of the obtained denoised image with the noisy image. The blind metrics are generally used for experimentally obtained images where access to ground truths are not possible. Here we have used three criteria metrics: *PSNR*, *Q*, and *EPI* for the assessment of the denoising methods for the simulated speckle fringe pattern and wrapped phase fringe pattern and the *SNR* for the reconstructed two-dice image.

The peak signal-to-noise ratio (PSNR) is defined as the ratio between the maximum possible power of a signal and the power of denoised noise, given by [12]

$$PSNR(f_{out}, f) = 10\log_{10}\left(\frac{L^2}{MSE(f_{out}, f)}\right) \qquad (12)$$

where $L=2^8-1=255$ is the maximal possible value of the image pixels when pixels are represented using 8-bits per sample, and MSE is the mean squared difference between the original image and denoised image, given by:

$$MSE(f_{out}, f) = \frac{1}{N.M}\sum_{i=1}^{N}\sum_{j=1}^{M}\left[f(i,j) - f_{out}(i,j)\right] \qquad (13)$$

with m and n are the number of pixels along horizontal and vertical direction respectively, $I(x_i, y_i)$ represents the pixel value at position (i, j) in the original image and $I_{out}(x_i, y_i)$ represents the pixel value at the same position in the corresponding denoised image. The PSNR value must be maximum as much as possible because the good image quality is associated with the higher PSNR value.

The quality index (Q) is defined as [12]:

$$Q = \frac{4\sigma_{xy}\langle f\rangle\langle f_{out}\rangle}{\left(\sigma_x^2+\sigma_y^2\right)\left(\left(\langle f\rangle\right)^2+\left(\langle f_{out}\rangle\right)^2\right)} \qquad (14)$$

where, μ_I and μ_{out} are the mean values of the images $I(x_i, y_i)$ and $I_{out}(x_i, y_i)$, σ_I and $\sigma_{I_{out}}$ are their variances, respectively, and $\sigma_{II_{out}}$ is their covariance. The value of Q is counted in the interval [−1, +1], when the two images are quite similar, then the value of Q approaches to +1 [12,39].

The edge preservation index (EPI) is defined as:

$$EPI = \frac{\sum_{i=1}^{m}\sum_{j=1}^{n-1}\left|f_{out}(i,j+1) - f_{out}(i,j)\right|}{\sum_{i=1}^{m}\sum_{j=1}^{n-1}\left|f(i,j+1) - f(i,j)\right|} \qquad (15)$$

EPI describes the edge preservation capability of the images obtained after the implementation of a denoising method. Higher the value of EPI, the more the preservation of the edges of the denoised image. Therefore, a reasonably high EPI value ensures a better visible image quality [12].

The PSNR, Q, and EPI metrics are based on ground truths in which the obtained denoised image is compared with its corresponding noise-free image. In the case of real data, the computation of these three metrics is impossible because they are not any reference image, so, we use the signal to noise ratio (SNR) defined as:

$$SNR = \frac{\sum_{i=0}^{m-1}\sum_{j=0}^{n-1} I_{out}(x_i, y_j)^2}{\sum_{i=0}^{m-1}\sum_{j=0}^{n-1}\left[I_{out}(x_i, y_j) - I(x_i, y_j)\right]^2} \qquad (16)$$

Low SNR value is the better quality of denoising.

These parameters are intensively used to evaluate the performance of the denoising methods to demonstrate better image/fringe pattern enhancement, restoration, and quality

of the perceived image/fringe pattern [12,39].

The obtaining PSNR, Q, and EPI values computed for airplane and building images are summarized in table 1 and table 2 respectively. According to table 1, the obtained PSNR, Q, and EPI values show that the proposed method effectively reduces speckle noise with high accuracy. This performance was found to be very promising when compared to the Frost filter, Lee filter, and NLM-SAR method.

The same promising results are obtained using building image (See table 2), and it can be noticed that despite the speckle variance increase, the proposed method give good results.

For the four speckle noise variance used in this study, the proposed method provides better denoising results in terms of PSNR and Q for the airplane and building image, highlighting that for the four speckle variance, the proposed method provides the high values for PSNR and Q. However, it is observed that with increasing speckle variance, the EPI values was provided with good results using NLM-SAR but just with a different ratio of 0.1%.

Table 1. PSNR, Q, AND EPI METRICS RESULTS FOR AIRPLANE IMAGE

	Proposed method			Frost filter			Lee filter			NLM-SAR		
Variance	**PSNR**	**Q**	**EPI**	**PSNR**	**Q**	**EPI**	**PSNR**	**Q**	**EPI**	**PSNR**	**Q**	**EPI**
0,05	30,512	0,93	0,953	21,881	0,872	0,921	21,429	0,922	0,962	28,814	0,921	0,992
0,1	29,201	0,911	0,948	21,611	0,868	0,911	21,245	0,915	0,95	28,547	0,911	0,987
0,2	28,015	0,882	0,941	21,54	0,812	0,901	20,656	0,9	0,953	27,068	0,88	0,981
0,3	27,15	0,823	0,902	20,376	0,752	0,898	20,251	0,894	0,917	25,603	0,819	0,977

Table 2. PSNR, Q, AND EPI METRICS RESULTS FOR BUILDING IMAGE

	Proposed method			Frost filter			Lee filter			NLM-SAR		
Variance	**PSNR**	**Q**	**EPI**	**PSNR**	**Q**	**EPI**	**PSNR**	**Q**	**EPI**	**PSNR**	**Q**	**EPI**
0,05	29,912	0,913	0,983	22,801	0,892	0,981	24,129	0,982	0,962	28,814	0,901	0,999
0,1	29,615	0,901	0,978	21,452	0,878	0,971	23,895	0,975	0,95	28,502	0,891	0,977
0,2	28,415	0,892	0,971	21,912	0,832	0,969	21,6	0,91	0,953	26,868	0,888	0,961
0,3	27,789	0,815	0,952	20,405	0,782	0,928	20,751	0,898	0,977	22,123	0,705	0,957

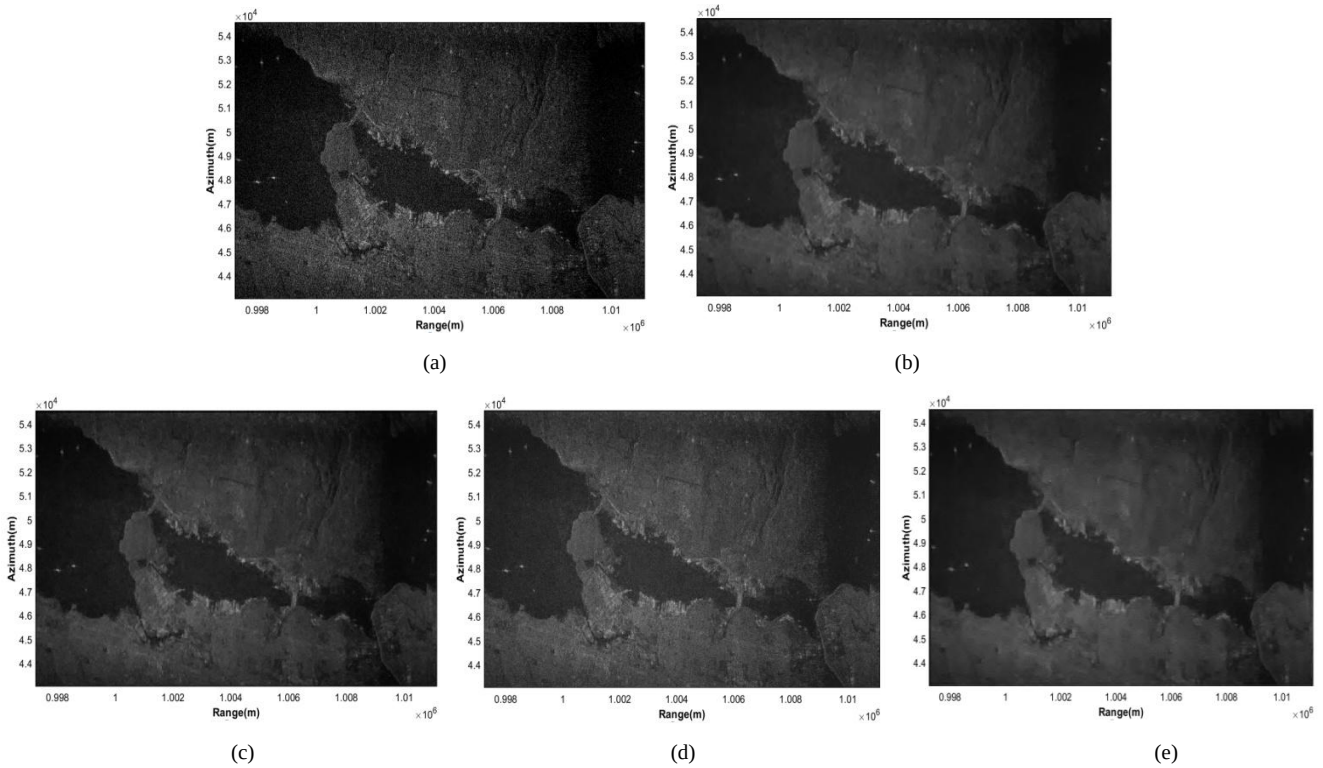

Figure 11. (a) Radarsat SAR image of Stanley Park-Vancouver City (**SNR=21.33 dB**), and Denoised image using: (b) the proposed method (**SNR=12.150 dB**), (c) Frost filter (**SNR=15.210 dB**), (d) Lee filter (**SNR=14.258 dB**) and (e) NLM-SAR method (**SNR=13.952 dB**)

3.3. Application to a Real SAR Image

After the validation of the proposed method by numerical simulation, a real SAR image of Stanley Park in Vancouver city acquired by the Radarsat-2 remote sensing satellite showed in Figure 11.a. Figure 11(b-e) show the obtained denoised image using the proposed method, Frost filter, Lee filter, and NLM-SAR method respectively. The input real SAR image has an SNR=21.33 dB, and this value decreases using the denoising methods and we found that our proposed method gives the low SNR value of 12.150 dB.

4. Conclusions

A new hybrid method for speckle noise reduction in SAR images was proposed in this paper. The method combines the two-dimensional variational mode decomposition and nonlocal means reprojection method using Box kernel with minimizing variance. After the decomposition of the input SAR image into series of high frequencies components, low-frequency components, and residue using 2D-VMD, the high-frequency components were denoised using the NLM Reprojection method. The simulation study shows that the obtained method improves the denoising quality more than other famous methods as Frost filter, Lee filter, and NLM-SAR method. The performance of the proposed method was also demonstrated using a real SAR image required by Radarsat. Overall, it can be concluded that the 2D-VMD/NLM-Reprojection method for speckle noise removing is effective and could be established as a powerful denoising method for SAR images, and therefore, facilitate the analysis and interpretation of SAR images.

REFERENCES

[1] F. Bovenga, « Special Issue “Synthetic Aperture Radar (SAR) Techniques and Applications” », Sensors, vol. 20, no 7, mars 2020, doi: 10.3390/s20071851.

[2] N. Yahya, N. S. Kamel, et A. S. Malik, « Subspace-Based Technique for Speckle Noise Reduction in SAR Images », IEEE Trans. Geosci. Remote Sens., vol. 52, no 10, p. 6257‑6271, oct. 2014, doi: 10.1109/TGRS.2013.2295824.

[3] F. Guo, G. Zhang, Q. Zhang, R. Zhao, M. Deng, et K. Xu, « Speckle Suppression by Weighted Euclidean Distance Anisotropic Diffusion », Remote Sens., vol. 10, no 5, Art. no 5, mai 2018, doi: 10.3390/rs10050722.

[4] L. Gemme et S. G. Dellepiane, « An Automatic Data-Driven Method for SAR Image Segmentation in Sea Surface Analysis », IEEE Trans. Geosci. Remote Sens., vol. 56, no 5, p. 2633‑2646, mai 2018, doi: 10.1109/TGRS.2017.2769710.

[5] Y. Yuan, J. Fang, X. Lu, et Y. Feng, « Remote Sensing Image Scene Classification Using Rearranged Local Features », IEEE Trans. Geosci. Remote Sens., vol. 57, no 3, p. 1779‑1792, mars 2019, doi: 10.1109/TGRS.2018.2869101.

[6] E. Shah, P. Jayaprasad, et M. E. James, « Image Fusion of SAR and Optical Images for Identifying Antarctic Ice Features », J. Indian Soc. Remote Sens., vol. 47, no 12, p. 2113‑2127, déc. 2019, doi: 10.1007/s12524-019-01040-3.

[7] Hua Xie, L. E. Pierce, et F. T. Ulaby, « Statistical properties of logarithmically transformed speckle », IEEE Trans. Geosci. Remote Sens., vol. 40, no 3, p. 721‑727, mars 2002, doi: 10.1109/TGRS.2002.1000333.

[8] X. Li, Y. Hu, X. Gao, D. Tao, et B. Ning, « A multi-frame image super-resolution method », Signal Process., vol. 90, no 2, p. 405‑414, févr. 2010, doi: 10.1016/j.sigpro.2009.05.028.

[9] L. G. Shapiro et G. C. Stockman, Computer Vision. Upper Saddle River, NJ: Pearson, 2001.

[10] C. Tomasi et R. Manduchi, « Bilateral filtering for gray and color images », in Sixth International Conference on Computer Vision (IEEE Cat. No.98CH36271), janv. 1998, p. 839‑846, doi: 10.1109/ICCV.1998.710815.

[11] A. Buades, B. Coll, et J.-M. Morel, « A non-local algorithm for image denoising », in 2005 IEEE Computer Society Conference on Computer Vision and Pattern Recognition (CVPR’05), juin 2005, vol. 2, p. 60‑65 vol. 2, doi: 10.1109/CVPR.2005.38.

[12] Y. Tounsi, M. Kumar, A. Nassim, F. Mendoza-Santoyo, et O. Matoba, « Speckle denoising by variant nonlocal means methods », Appl. Opt., vol. 58, no 26, p. 7110‑7120, sept. 2019, doi: 10.1364/AO.58.007110.

[13] H. Wang, « SAR Image Denoising Based on Dual Tree Complex Wavelet Transform », in Computer Science for Environmental Engineering and EcoInformatics, Berlin, Heidelberg, 2011, p. 430‑435, doi: 10.1007/978-3-642-22691-5_75.

[14] A. Nassim, Y. Tounsi, et A. Siari, Denoising in digital speckle pattern interferometry by Riesz wavelets. LAP LAMBERT Academic Publishing, 2018.

[15] T. Yassine, S. Ahmed, et N. Abdelkrim, « Speckle noise reduction in digital speckle pattern interferometry using Riesz wavelets transform », in 2017 International Conference on Advanced Technologies for Signal and Image Processing (ATSIP), mai 2017, p. 1‑4, doi: 10.1109/ATSIP.2017.8075565.

[16] A. Misra, B. Kartikeyan, et S. Garg, « Wavelet based SAR data denoising and analysis », in 2014 IEEE International Advance Computing Conference (IACC), févr. 2014, p. 1087‑1092, doi: 10.1109/IAdCC.2014.6779477.

[17] H. Choi et J. Jeong, « Speckle Noise Reduction Technique for SAR Images Using Statistical Characteristics of Speckle Noise and Discrete Wavelet Transform », Remote Sens., vol. 11, no 10, Art. no 10, janv. 2019, doi: 10.3390/rs11101184.

[18] Q. Kemao, « Two-dimensional windowed Fourier transform for fringe pattern analysis: Principles, applications and implementations », Opt. Lasers Eng., vol. 45, no 2, p. 304‑317, févr. 2007, doi: 10.1016/j.optlaseng.2005.10.012.

[19] H. Fattahi, M. J. V. Zoej, M. R. Mobasheri, M. Dehghani, et M. R. Sahebi, « Windowed Fourier Transform for Noise Reduction of SAR Interferograms », IEEE Geosci. Remote Sens. Lett., vol. 6, no 3, p. 418‑422, juill. 2009, doi: 10.1109/LGRS.2009.2015338.

[20] C. Yue et W. Jiang, « SAR image denoising in nonsubsampled contourlet transform domain based on maximum a posteriori and non-local constraint », Remote Sens. Lett., vol. 4, no 3, p. 270‑278, mars 2013, doi: 10.1080/2150704X.2012.723146.

[21] J. M. Mejía Muñoz et al., « SAR Image Denoising Using the Non-Subsampled Contourlet Transform and Morphological Operators », in Advances in Artificial Intelligence, Berlin, Heidelberg, 2010, p. 337‑347, doi: 10.1007/978-3-642-16761-4_30.

[22] J. Hu, Y. Li, et Y. Jia, « Automatic SAR Image Enhancement Based on Curvelet Transform and Genetic Algorithm », in Intelligent Science and Intelligent Data Engineering, Berlin, Heidelberg, 2012, p. 326‑333, doi: 10.1007/978-3-642-31919-8_42.

[23] J. R. Sveinsson et J. A. Benediktsson, « Combined wavelet and curvelet denoising of SAR images using TV segmentation », in 2007 IEEE International Geoscience and Remote Sensing Symposium, juill. 2007, p. 503‑506, doi: 10.1109/IGARSS.2007.4422841.

[24] E. Dalsasso, X. Yang, L. Denis, F. Tupin, et W. Yang, « SAR Image Despeckling by Deep Neural Networks: from a Pre-Trained Model to an End-to-End Training Strategy », Remote Sens., vol. 12, no 16, Art. no 16, janv. 2020, doi: 10.3390/rs12162636.

[25] H. Imad, T. Yassine, B. Mohammed, et N. Abdelkrim, « Batch despeckling of SAR images by a convolutional neural network-based method », in 2020 IEEE International conference of Moroccan Geomatics (Morgeo), mai 2020, p. 1‑6, doi: 10.1109/Morgeo49228.2020.9121890.

[26] M. Rahimi et M. Yazdi, « A new hybrid algorithm for speckle noise reduction of SAR images based on mean-median filter and SRAD method », in 2015 2nd International Conference on Pattern Recognition and Image Analysis (IPRIA), mars 2015, p. 1‑6, doi: 10.1109/PRIA.2015.7161623.

[27] B. Marhaba et M. Zribi, « Reduction of Speckle Noise in SAR Images Using Hybrid Combination of Bootstrap Filtering and DWT », in 2018 International Conference on Computer and Applications (ICCA), août 2018, p. 377‑382, doi: 10.1109/COMAPP.2018.8460380.

[28] A. Nassim, Y. Tounsi, et A. Siari, Denoising in digital speckle pattern interferometry by Riesz wavelets. LAP LAMBERT Academic Publishing, 2018.

[29] T. Yassine, S. Ahmed, et N. Abdelkrim, « Speckle noise reduction in digital speckle pattern interferometry using Riesz wavelets transform », in 2017 International Conference on Advanced Technologies for Signal and Image Processing (ATSIP), mai 2017, p. 1-4, doi: 10.1109/ATSIP.2017.8075565.

[30] K. Dragomiretskiy et D. Zosso, « Variational Mode Decomposition », IEEE Trans. Signal Process., vol. 62, no 3, p. 531‑544, févr. 2014, doi: 10.1109/TSP.2013.2288675.

[31] Z. Wu, N. E. Huang, S. R. Long, et C.-K. Peng, « On the trend, detrending, and variability of nonlinear and nonstationary time series », Proc. Natl. Acad. Sci., vol. 104, no 38, p. 14889‑14894, sept. 2007, doi: 10.1073/pnas.0701020104.

[32] Y. Wang, R. Markert, J. Xiang, et W. Zheng, « Research on variational mode decomposition and its application in detecting rub-impact fault of the rotor system », Mech. Syst. Signal Process., vol. 60‑61, p. 243-251, août 2015, doi: 10.1016/j.ymssp.2015.02.020.

[33] B. He et Y. Bai, « Signal-noise separation of sensor signal based on variational mode decomposition », in 2016 8th IEEE International Conference on Communication Software and Networks (ICCSN), juin 2016, p. 132-138, doi: 10.1109/ICCSN.2016.7586634.

[34] K. Dragomiretskiy et D. Zosso, « Two-Dimensional Variational Mode Decomposition », in Energy Minimization Methods in Computer Vision and Pattern Recognition, Cham, 2015, p. 197‑208, doi: 10.1007/978-3-319-14612-6_15.

[35] J. Salmon et Y. Strozecki, « From patches to pixels in Non-Local methods: Weighted-average reprojection », in 2010 IEEE International Conference on Image Processing, sept. 2010, p. 1929‑1932, doi: 10.1109/ICIP.2010.5650780.

[36] V. S. Frost, J. A. Stiles, K. S. Shanmugan, et J. C. Holtzman, « A Model for Radar Images and Its Application to Adaptive Digital Filtering of Multiplicative Noise », IEEE Trans. Pattern Anal. Mach. Intell., vol. PAMI-4, no 2, p. 157‑166, mars 1982, doi: 10.1109/TPAMI.1982.4767223.

[37] J.-S. Lee, « Digital Image Enhancement and Noise Filtering by Use of Local Statistics », IEEE Trans. Pattern Anal. Mach. Intell., vol. PAMI-2, no 2, p. 165‑168, mars 1980, doi: 10.1109/TPAMI.1980.4766994.

[38] S. Parrilli, M. Poderico, C. V. Angelino, G. Scarpa, et L. Verdoliva, « A nonlocal approach for SAR image denoising », in 2010 IEEE International Geoscience and Remote Sensing Symposium, juill. 2010, p. 726-729, doi: 10.1109/IGARSS.2010.5651432.

[39] M. Kumar, Y. Tounsi, K. Kaur, A. Nassim, F. Mandoza-Santoyo, et O. Matoba, « Speckle denoising techniques in imaging systems », J. Opt., vol. 22, no 6, p. 063001, mai 2020, doi: 10.1088/2040-8986/ab8b7f.